

## Article

# The Influence of Assembly Unit of Fibers on the Mechanical and Long-Term Properties of Reactive Powder Concrete

Zhangjie Cai <sup>1</sup>, Jie Ren <sup>2</sup>, Guangming Shen <sup>3</sup>, Changhong Jin <sup>2</sup>, Xingqing Gu <sup>4</sup>, Wenjie Cheng <sup>1</sup> and Hui Wang <sup>5,\*</sup><sup>1</sup> Civil Engineering Department, Yancheng Institute of Technology, Yancheng 224051, China<sup>2</sup> China Construction Infrastructure Co., Ltd., Beijing 100029, China<sup>3</sup> Jiuzhou Engineering Design Co., Ltd., Zhengzhou 451162, China<sup>4</sup> College of Civil Aviation, Nanjing University of Aeronautics and Astronautics, Nanjing 210016, China<sup>5</sup> School of Civil Engineering and Geographic Environment, Ningbo University, Ningbo 315000, China

\* Correspondence: huiwang123@aliyun.com

**Abstract:** The corrosion of concrete structures by chloride salt is very significant in coastal environments. In order to improve the durability of marine concrete structures, cement-based materials with high durability need to be developed. In this investigation, the influence of NaCl freeze–thaw cycles (FT-C) and NaCl dry-wet alternations (DW-A) on the flexural and compressive strengths of reactive powder concrete (RPC) with an assembly unit of basalt fibers and steel fibers is studied. Additionally, the mass loss rate, the relative dynamic modulus of elasticity (RDEM), the chloride ion migration coefficient (CMC) and the impact toughness are measured after the NaCl FT-C and DW-A action. Our findings show that the RDEM, mass loss, and mechanical strength loss of RPC are increased by the ascending NaCl FT-C and DW-A. Meanwhile, the RDEM and the impact toughness are decreased by the NaCl FT-C and DW-A. The RPC with 0.5% basalt fibers and 1.5% steel fibers by volume of RPC shows the optimum mechanical performance and resistance to NaCl FT-C and DW-A. However, RPC with 3% steel fibers shows the worst resistance to NaCl erosion. The maximum mass loss rates, RDEM, flexural strength loss rate, compressive strength loss rate, CMC and impact toughness of all specimens after 300 NaCl FT-C and 30 NaCl DW-A are 4.5%, 91.7%, 28.1%, 29.3%,  $3.2 \times 10^{-12}$  (m<sup>2</sup>/s) and 2471 J. Meanwhile, the corresponding minimum values are 1.62%, 83.2%, 20.4%, 15.7%,  $1.1 \times 10^{-12}$  (m<sup>2</sup>/s) and 625 J. The researching findings will provide an optimum mix ratio of RPC with an assembly unit of basalt fibers and steel fibers, which can be applied in the marine engineering environment.

**Keywords:** mechanical strength; assembly unit; basalt fibers; steel fibers; reactive powder concrete; NaCl erosion action; impact toughness



**Citation:** Cai, Z.; Ren, J.; Shen, G.; Jin, C.; Gu, X.; Cheng, W.; Wang, H. The Influence of Assembly Unit of Fibers on the Mechanical and Long-Term Properties of Reactive Powder Concrete. *Coatings* **2023**, *13*, 412. <https://doi.org/10.3390/coatings13020412>

Academic Editor: Andrea Nobili

Received: 27 January 2023

Revised: 6 February 2023

Accepted: 10 February 2023

Published: 11 February 2023



**Copyright:** © 2023 by the authors. Licensee MDPI, Basel, Switzerland. This article is an open access article distributed under the terms and conditions of the Creative Commons Attribution (CC BY) license (<https://creativecommons.org/licenses/by/4.0/>).

## 1. Introduction

Cement concrete is one of the most widely used materials [1,2]. Reactive powder concrete (RPC) is a kind of cement-based material which is manufactured with cement, mineral admixtures, quartz sand, water and high-performance water-reducing agent (WRA) [3,4]. This kind of material shows high compactness and mechanical performance. When the cement concrete is used in the coastal urban environment, serious deterioration in the concrete occurs. For coastal civil engineering construction materials, the chloride erosion effect is the most severe. Ordinary cement concrete is prone to corrosion during service in the marine environment. Meanwhile, the application of RPC can improve the service life of construction buildings [5–9].

Steel fibers, plant fibers, basalt fibers, carbon fibers, and carbon nanotubes have been applied in reinforcing the performance of RPC. However, steel fibers are easy to corrode when applied in the marine environment [10,11]. The freeze–thaw cycles and dry-wet alternations of seawater can accelerate the deterioration of cement concrete [12–14]. When the steel fibers are mixed in RPC, the corroded steel fibers can induce more serious cracks in

the cement concrete, thus decreasing the mechanical performance of cement concrete. The carbon fibers and carbon nanotubes show positive excellent corrosion resistance [15–17]. These fibers are extremely expensive, and not suitable for application in cement-based materials. The plant fibers shows low cost and good corrosion resistance. However, their reinforcing effect on mechanical performance is limited.

Basalt fiber is a kind of continuous fiber manufactured by natural basalt after melting in a high temperature environment of 1450~1500 °C and drawing at high speed through a platinum rhodium alloy wire drawing bushing. The tensile ratio of basalt fiber is as high as 15%~18%, which can be uniformly distributed in cement concrete. The addition of basalt fibers can prevent the sink of aggregate and improve the uniformity of RPC. Moreover, the segregation can be decreased and the workability can be improved through the addition of basalt fibers [18–20]. Additionally, the tensile strain of cement concrete can be limited by basalt fibers; meanwhile, concrete shrinkage can be decreased by basalt fibers. Li et al. [2], reported that 0.5% of the total volume of RPC is the optimum fiber volume of basalt fibers. Furthermore, basalt fibers can effectively improve the impact toughness and provide excellent resistance to freeze–thaw and carbonation of RPC. The copper-plated fine steel fibers exhibit high corrosion resistance and perfect mechanical performance. The RPC with an assembly unit of basalt fibers and copper-plated fine steel fibers may exhibit better mechanical and durable properties. However, little attention has been paid to the effect of NaCl erosion on the performances of RPC with assembly units of basalt fibers and copper-plated fine steel fibers [21,22].

In this study, the mass loss rate, the relative dynamic modulus of elasticity (RDME), the flexural loss rate, the compressive strength loss rate and the impact toughness of RPC with an assembly unit of basalt fibers and copper-plated fine steel fibers are measured. Freeze–thaw cycles (FT-C) and the dry-wet alternations (DW-A) of NaCl are exerted on the RPC specimens. This research will provide a new high-performance concrete material which may be applicable to coastal environment.

## 2. Materials and Methods

### 2.1. Raw Materials

Ordinary Portland cement (OPC) provided by Aosheng Construction Co., Ltd., Yanchen, China is selected. The cement has a density of 3.05 g/cm<sup>3</sup>, a compressive strength of 42.5 MPa, and an initial setting time and final setting time of 107 min and 361 min. The blast furnace slag (BFS) shows a density of 2.89 g/cm<sup>3</sup>, a specific surface area of 437.5 m<sup>2</sup>/g and a thermogravimetric loss rate of 2.3%. Silica fume (SF) with a specific surface area and density of 15 m<sup>2</sup>/g and 2.2 g/cm<sup>3</sup> is used for this research. SF is produced by the Shanggao Mingzheng Plastic Factory, Yichun, China. Meanwhile, the ultra-fine fly ash (FA) exhibits a density of 2.11 g/cm<sup>3</sup> and a specific surface area of 387 m<sup>2</sup>/g. The chemical composition and the particle size distributions of the binder materials are shown in Tables 1 and 2. Quartz sand with particle sizes of 1.1~0.70 mm, 0.61~0.34 mm and 0.148~0.298 mm is used as the aggregate in this experiment. Liquid poly-carboxylic acid water-reducing agent (WRA) with a 40% water-reducing rate is used for adjusting the working performance of fresh RPC paste. Calcium formate, polyether surfactants and dry powdered DF-04 defoamer are used as early strength agent and defoamer. Basalt fibers (BFs) with excellent acid and alkali resistance are provided by Shandong Taicheng Fiber Factory, Taian, China, showing a density of 2.71 g/cm<sup>3</sup>, a length of 15–18 mm, and a diameter of 18–48 μm, a the fracture strength of 1050 MPa, and an average modulus of elasticity of 3781 MPa. Copper-plated steel fibers (SFs), offered by Anshan Cobit, Anshan, China, with an average length of 1.5 cm, a diameter of 0.2 mm, a density of 7.85 g/cm<sup>3</sup> and a tensile strength of 2812 MPa are used in the measurement.

**Table 1.** Particle passing percentage of raw materials (%).

Types' Particle Size (%)	0.3 $\mu\text{m}$	0.6 $\mu\text{m}$	1 $\mu\text{m}$	4 $\mu\text{m}$	8 $\mu\text{m}$	64 $\mu\text{m}$	360 $\mu\text{m}$
OPC	0	0.3	2.7	15.0	28.8	93.6	100
BFS	0.04	0.11	3.6	19.7	35.1	98.0	100
Sand	0.01	0.02	0.02	0.02	0.04	20	100
FA	12.3	41.7	66.2	100	100	100	100
SF	31.3	58.4	82.2	94.6	99.4	99.4	100

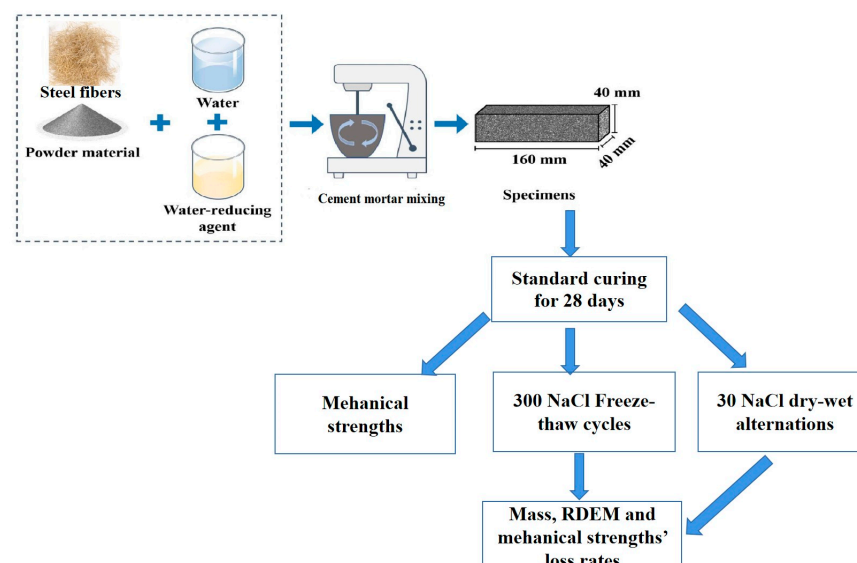
**Table 2.** The compositions (%).

Types' Compositions	SiO <sub>2</sub>	Al <sub>2</sub> O <sub>3</sub>	Fe <sub>x</sub> O <sub>y</sub>	MgO	CaO	SO <sub>3</sub>	K <sub>2</sub> O	Na <sub>2</sub> O	Ti <sub>2</sub> O	Loss on Ignition
OPC	20.9	5.5	3.9	1.7	62.2	2.7	-	-	-	3.1
BFS	34.1	14.7	0.2	9.7	35.9	0.2	3.5	-	-	-
Sand	99.6	-	0.02	-	-	-	-	-	-	-
FA	55.00	20.00	6.00	10.20	4.50	0.11	1.26	2.13	0.06	0.74
SF	90.0	0.2	0.6	0.2	0.4	0	7.4	-	-	-

## 2.2. Sample Preparation and Measurement Methods

### 2.2.1. Sample Manufacturing

The samples are prepared with the mixing proportions shown in Table 3, including water, OPC, FA, SF, BFS, quartz sand, WR, BFs and SFs. All dry powder materials are mixed in a UJZ-15 mortar mixer for 30 s. Then, the steel fibers and basalt fibers are mixed evenly in the dry materials for another 30 s. Finally, the water-reducing agent and water are stirred uniformly for the last 5 min. After the stirring, the fresh RPC paste is poured, forming specimens with sizes of  $40 \times 40 \times 160 \text{ mm}^3$ ,  $100 \times 100 \times 400 \text{ mm}^3$  and  $\Phi 100 \times 50 \text{ mm}^3$ . All the specimens are cured in the standard curing environment for 28 days before measurement. The standard curing environment can be divided into two steps. Firstly, specimens are cured in the environment with a temperature of  $20 \pm 2 \text{ }^\circ\text{C}$  and a relative humidity of 60% for 1 day before demolding. Then, the specimens are moved to the standard curing room with a temperature of  $20 \pm 2 \text{ }^\circ\text{C}$  and a relative humidity of  $98\% \pm 1\%$ . Figure 1 shows the manufacturing and measuring processes.

**Figure 1.** The manufacturing and measuring processes.

**Table 3.** Mix proportion of RPC per unit volume (kg/m<sup>3</sup>).

Water	OPC	FA	SF	BFS	Sand	WR	BFs	SFs
183.3	740.7	148.12	222.18	111.1	977.9	16.3	0	157
183.3	740.7	148.12	222.18	111.1	977.9	16.3	0	235.5
183.3	740.7	148.12	222.18	111.1	977.9	16.3	54.2	0
183.3	740.7	148.12	222.18	111.1	977.9	16.3	81.3	0
183.3	740.7	148.12	222.18	111.1	977.9	16.3	13.55	117.75

### 2.2.2. Measurement of Mechanical Strengths

Specimens with a size of  $40 \times 40 \times 160 \text{ mm}^3$  are made for measuring the flexural and compressive strengths. The mechanical strengths are measured with a YDW-100C microcomputer full-automatic universal tester provided by Jinan Xulian Instrument and Equipment Co., Ltd., Jinan, China. The loading speeds for the flexural and compressive strengths are 0.05 and 2.4 kN/s. Figure 2 shows the measuring process of flexural and compressive strengths.

**Broken specimens****Crushed specimens****Figure 2.** The measuring process of flexural and compressive strengths.

### 2.2.3. Measurement of Impact Toughness

The JLW-100 drop weight impact test measured impact toughness. The test method proposed by the American Concrete Institute (ACI) 544 committee is used to measure the impact toughness of concrete beams. The specimen is  $100 \times 100 \times 400 \text{ mm}^3$  in size, the drop hammer weighs 1.5 kg, the clear span of the beam is 360 mm, and the span of the upper loading section is 120 mm.

A four-point loading mode is adopted to apply impact load on the specimen. The measuring equipment is exhibited in Figure 3. In the study, three replicates are used for each group. The average impact toughness is considered as the index of concrete impact resistance. The strain gauge is fixed at the axial position of the bottom center of the beam, and the dynamic strain gauge is used to monitor the concrete. If a sudden increase in strain happens during impact, cracks may start to generate in the beam. With an increase in impact times, the number of impact times virtually stays the same. The impact toughness can be calculated by Equation (1).

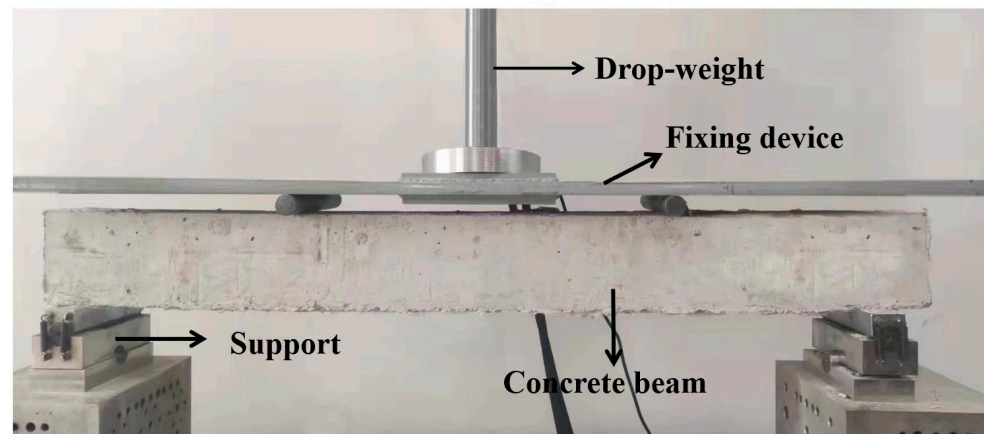


**Figure 3.** The test process and loading mode of the impact test.

The specimen is simply supported, and its calculated span is 340 mm. In this section, the impact toughness index and impact energy dissipation performance of different beams are obtained using a drop weight bending impact test for nine groups of different mixing proportions.

In this impact test, a 2.5 kg drop hammer (5 kg rod weight) is used to impact the side of the forces specimen from a height of 400 mm. The crack propagation width of the specimen surface is observed by the specimens' crack width detector (as shown in Figure 2), which is used to determine the impact times at the initial crack. The impact test is repeated until the specimen fails.

The impact toughness index ( $\beta$ ) for drop hammer impact testing is defined as the ratio of the difference between the failure impact number ( $N_2$ ) and the initial crack impact number ( $N_1$ ) to the initial crack impact number ( $N_1$ ). The impact toughness index represents the ratio of the impact energy consumption after the crack appears to the impact energy consumption before the initial crack, and reflects the toughness of the material after the crack. Among them, the impact times of the initial crack are the initial stage of impact. For each test, the experimental steps are carried out as follows. Firstly, the bottom of the specimen is wiped with alcohol, and then the impact times are recorded and detected. The impact times of failure are recorded as soon as the crack width detector identifies the first crack that has a width of 0.05 mm. In the whole impact test, the impact energy consumption ( $W$ ) of the specimen is the work accumulation of each impact. It can be calculated as follows:

$$W = mghN \quad (1)$$

where  $N$  represents the total number of impact failures,  $m$  notes the mass of the whole drop-weight, which in this study is 7.5 kg,  $h$  is the dropping height, in this case 400 mm,  $g$  stands for gravitational acceleration, in this case  $9.8 \text{ m/s}^2$ . The impact toughness index ( $\beta$ ) can be calculated by Equation (2) as follows:

$$\beta = (N_2 - N_1) / N_1 \quad (2)$$

#### 2.2.4. NaCl Erosion Environment

Previously, NaCl (FT-C) and NaCl (DW-A) specimens with sizes of  $40 \times 40 \times 100 \text{ mm}^3$  were immersed in 3% NaCl solution for 4 days after standard curing for 24 days. Then, the specimens are subjected to the experiments of NaCl FT-C by the concrete rapid FT-C test box. A DW-A can be described following these steps. The specimens immersed in NaCl solution for 4 days are air dried at room temperature for 2 h. Then, the specimens are dried in the vacuum drying oven for 36 h and moved to room temperature and cooled for 2 h. Finally, all specimens are immersed in NaCl solution for the residual 10 h.

### 3. Results and Discussion

#### 3.1. Action of NaCl FT-C

##### 3.1.1. Mass Loss Rate and RDEM after Different NaCl FT-C

Figure 4 shows the mass loss rate of specimens during FT-C. It can be observed from figure that the mass loss rate of RPC increases with the increasing number of FT-C. The mass loss rate of RPC with 2% steel fibers is lower than that of RPC with 3% steel fibers. Meanwhile, the RPC with 3% basalt fibers shows a lower mass loss rate than the RPC with 2% basalt fibers and 3% steel fibers, but higher than that with 2% steel fibers. The RPC with an assembly unit of basalt fibers and steel fibers shows the lowest mass loss rate of all mix proportions. The main reason for this result is that the frost-heaving stress inside the RPC and the crystallization stress of NaCl during freezing and thawing cycles cause the RPC to bulge and crack, resulting in peeling. Therefore, the mass of RPC continues to decline during freezing and thawing. However, excessive steel fibers (3%) can accelerate the corrosion of steel fibers, and the corroded steel fiber is prone to cause cracking and peeling of RPC, thus accelerating its mass loss. Therefore, when the steel fiber content is 3%, the mass loss rate of RPC is the highest. The reinforcement effect of RPC mixed with 0.5% basalt fiber and 1.5% steel fiber is the best, leading to an optimum crack resistance effect of RPC. Consequently, the mass loss rate of RPC during FT-C is the smallest. The mass loss rates after 300 FT-C vary from 1.62%~4.5%. It can be observed from Figure 4 that the mass loss of RPC is less than 5%, which indicates that this type of RPC has excellent anti-NaCl freeze–thaw effect [23].

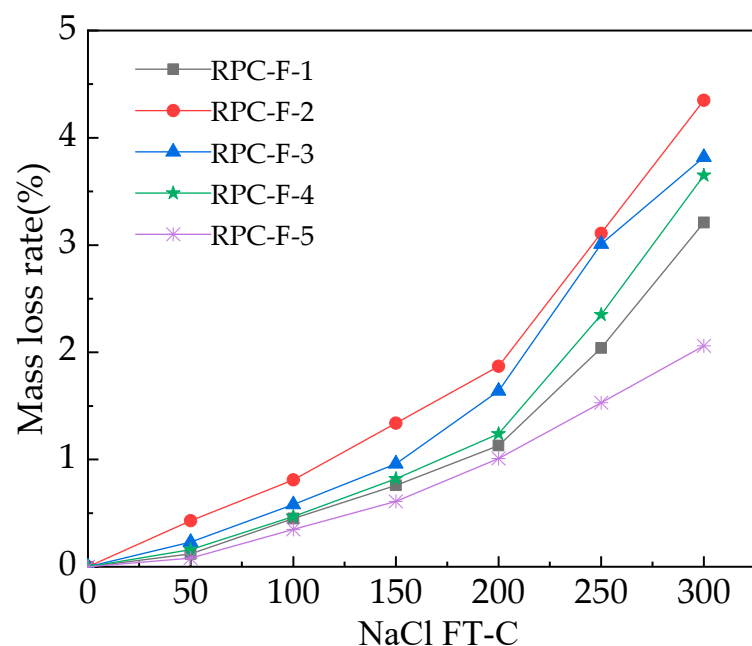
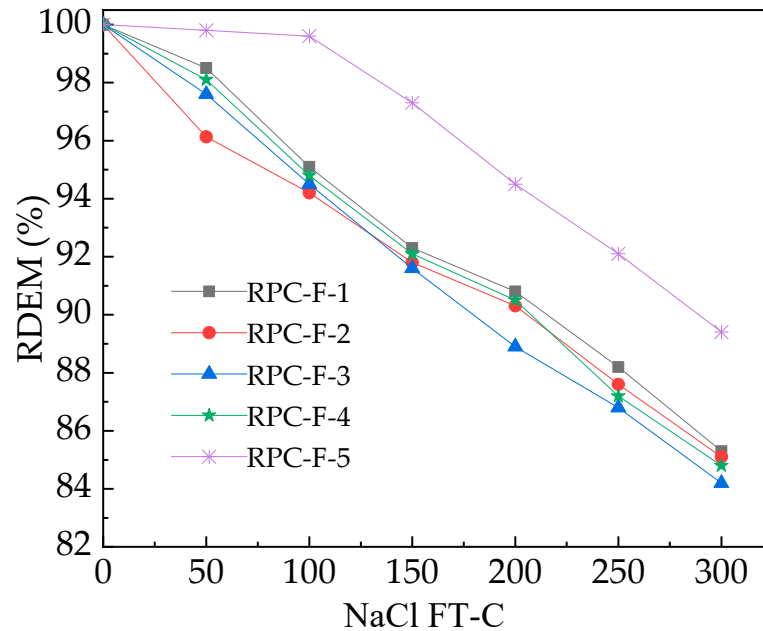


Figure 4. Mass loss rate during NaCl FT-C.

The relative dynamic modulus of elasticity (RDME) after exposure to a different number of FT-C is shown in Figure 5. As illustrated in Figure 5, the RDME decreases with the increasing FT-C. This is mainly because the cracks in the inner RPC increase with the increase of FT-C, and therefore the RDME of RPC decreases gradually during FT-C [24]. After suffering FT-C, the RDME is in accordance with the following order: 0.5% basalt fiber + 1.5% steel fiber RPC > 2% steel fiber RPC > 2% steel fiber RPC > 3% steel fiber RPC > 3% basalt fiber RPC > 2% basalt fiber RPC. This is due to the fact that the reinforcing effect of steel fibers on RPC is higher than that of basalt fibers, and the RDME of steel fiber-reinforced RPC with the same content is higher than that of the RPC with basalt fibers [25]. However, steel fibers will rust under the action of NaCl FT-C, which will cause acceleration of cracking, thus reducing the RDME of RPC. The fiber-reinforced effect of

the RPC mixed with 0.5% basalt fibers and 1.5% steel fibers is the best, hence the RDME of RPC is the highest at this time. The RDME after 300 NaCl FT-C ranges from 84.1%~91.7%, which is higher than 80%, thus showing excellent resistance to NaCl FT-C.



**Figure 5.** The RDEM of RPC during NaCl FT-C.

### 3.1.2. Mechanical Strength Loss Rates after NaCl FT-C

Figure 6 shows the flexural strength and compressive strength loss rates after different NaCl FT-C. It can be observed from Figure 6 that the mechanical strength loss rates of RPC gradually increase with the ascending number of FT-C. The mechanical strength loss rates of all specimens increase in the following order: RPC with 0.5% basalt fibers + 1.5% steel fibers < RPC with 2% steel fibers < RPC with 3% basalt fibers < RPC with 2% basalt fibers < RPC with 3% steel fibers. This is because the increased cracks during the FT-C lead to decreased mechanical strength [26]. Therefore, the increased number of FT-C will cause a continuous decrease in RPC strength. We can see from our results that a certain number of steel fibers and basalt fibers can enhance the mechanical and resistance of FT-C. However, excessive steel fibers will aggravate their corrosion, thus reducing the tensile property of steel fiber and leading to the reduction in mechanical strength. Additionally, steel fibers' corrosion leads to RPC expansion cracking, further reducing the mechanical strength. The assembly unit of basalt fibers and steel fibers possesses the advantages of two kinds of fibers, thus weakening their shortcomings. Therefore, the mechanical strength loss of RPC with 0.5% basalt fiber + 1.5% steel fiber is at a minimum. It can be seen in Figure 6 that the loss of compressive strength is lower than the flexural strength loss. This is because the cracks of RPC increase and widen due to FT-C. The crack growth rate of RPC in tension is higher than that in compression. Therefore, the reduction rate of flexural strength is higher than that of compressive strength. The flexural and compressive strengths loss rates are 22.3%~36.7% and 15.7%~28.1%.

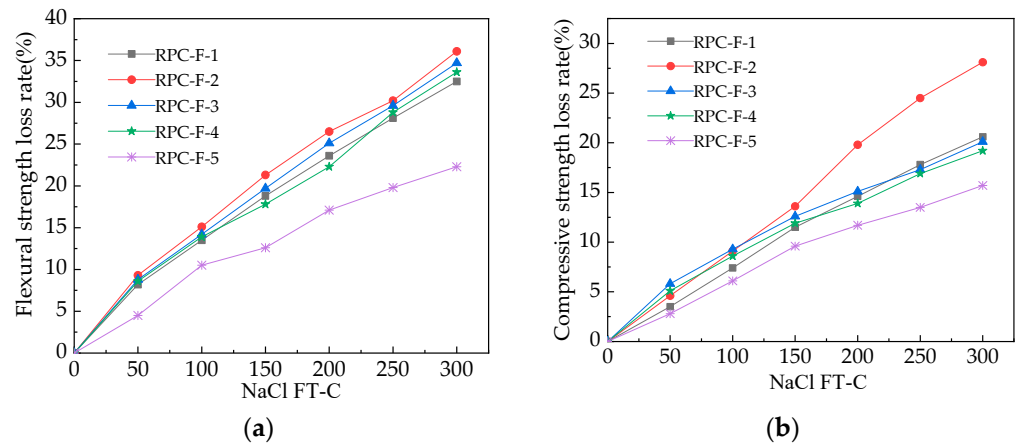


**Figure 6.** Mechanical strength loss rates after NaCl FT-C. (a) Flexural strength loss rate (b) Compressive strength loss rate.

### 3.1.3. CMC during NaCl FT-C

The CMC of RPC during different FT-C is exhibited in Figure 7. It can be seen in Figure 7 that the CMC decreases in the following order: RPC with 3% steel fibers > RPC with 2% steel fibers > RPC with 2% basalt fibers > RPC with 0.5% basalt fibers + 1.5% steel fibers, before the NaCl FT-C. As shown in Figure 7, the CMC descends obviously with the increasing number of NaCl FT-C. This is mainly ascribed to the fact that the cracking expansion of RPC is accelerated by the FT-C, leading to an increase in the CMC. Consequently, the CMC of RPC increases with the increasing FT-C [27]. After the FT-C, the CMC descends in the same order as that before NaCl FT-C. The CMC after 300 FT-C ranges from  $1.1 \times 10^{-12}$  ( $m^2/s$ )~ $3.2 \times 10^{-12}$  ( $m^2/s$ ).

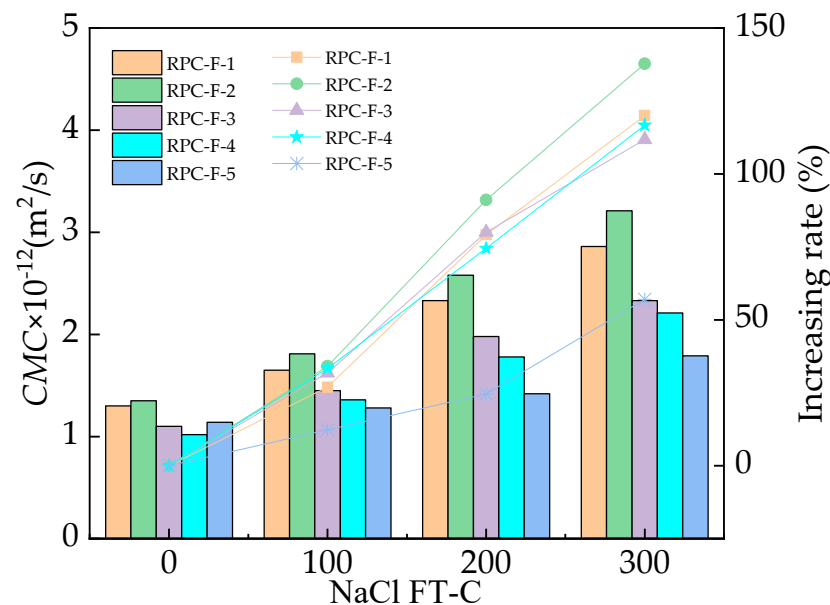


**Figure 7.** The CMC of RPC during NaCl FT-C.

### 3.1.4. Impact Toughness during NaCl FT-C

Figure 8 shows the impact toughness of RPC after different NaCl FT-C. As depicted in Figure 8, the initial impact toughness (impact toughness before NaCl corrosion) of RPC increases with the increasing fiber contents. The RPC with steel fibers shows higher impact toughness than the RPC with basalt fibers. This is mainly attributed to the fact that the fibers can consume the impact energy during the impact process. Besides, the fibers' pullout effect limits the extension of RPC cracks during impact; therefore, the impact toughness of RPC

is increased by adding fibers [28]. Meanwhile, the tensile toughness of steel fibers is higher than that of basalt fibers, leading to the result that the RPC with steel fibers shows higher impact toughness than the RPC with basalt fibers. RPC with 0.5% basalt fibers + 1.5% steel fibers performs the highest impact toughness. This is because this combination of fibers performs the highest the mechanical strength and the fiber dispersion, thus improving the impact toughness [29]. Moreover, as depicted in Figure 8, increasing NaCl FT-C results in decreasing impact toughness. This is attributed to increased cracks in the inner RPC during NaCl FT-C action [30]. Hence, the impact toughness is reduced by the NaCl FT-C. The impact toughness of RPC after being subjected to NaCl FT-C decreases in the following order: RPC with 3% steel fibers > 2% steel fibers RPC > 2% basalt fibers RPC > 3% basalt fibers > 0.5% basalt fibers mixed with 1.5% steel fiber RPC. When 300 NaCl FT-C are finished, the impact toughness is 625~2456 J.

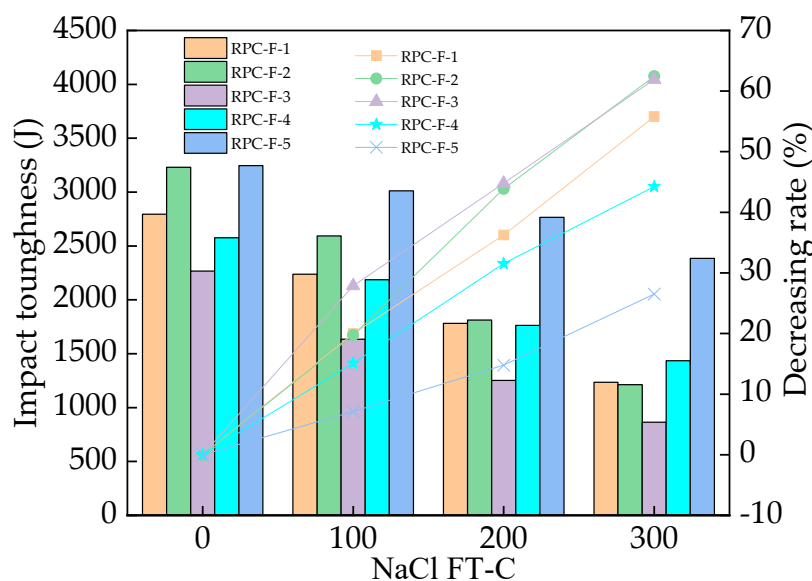


**Figure 8.** The impact toughness of RPC during NaCl FT-C.

Comparing our results with those of other researchers [25,27], the mass loss rates, RDEM, mechanical strengths loss rates and CMC of RPC with an assembly unit of steel fibers and basalt fibers after 300 NaCl FT-C are 77.1%~85.3%, 118.4%~126.7%, 82.5%~86.2%, and are 91.1%~92.3% in the RPC with mono-doped basalt fibers or steel fibers.

### 3.2. Action of NaCl DW-A

#### 3.2.1. Mass Loss Rate and RDEM after Different NaCl DW-A

The mass loss rates of RPC specimens after exposure to 0, 10, 20 and 30 NaCl DW-A are shown in Figure 9. As depicted in Figure 9, the mass loss rates of RPC increase with the rising number of DW-A. This is mainly due to the fact that NaCl will continuously crystallize and precipitate when the NaCl DW-A are exerted on the specimens [31]. As a result, the internal cracking and surface peeling of RPC will increase the mass loss of RPC. As found in Figure 9, the mass loss rates increase in the following order: RPC with 0.5% basalt fibers + 1.5% steel fibers < RPC with 2% steel fibers < RPC with 3% basalt fibers < RPC with 2% basalt fibers < RPC with 3% steel fibers. This is mainly because the addition of basalt fibers and steel fibers can limit crack propagation in the inner RPC, while steel fiber has a stronger limiting ability. However, during the process of DW-A, more  $\text{Cl}^-$  and  $\text{O}_2$  will enter the RPC to accelerate the corrosion of steel fibers, thus accelerating the crack propagation and peeling of the RPC [32]. Therefore, RPC with 3% steel fibers has the highest mass loss rate. Compared with steel fibers, basalt fibers have higher corrosion resistance. Therefore, the assembly unit of steel fibers and basalt fibers combine the advantages of the excellent mechanical properties of steel fibers and the high corrosion

resistance of basalt fibers. Consequently, the RPC with 0.5% basalt fibers + 1.5% steel fibers shows the lowest mass loss rate. The mass loss rate after 30 NaCl DW-A is 2.1%~3.2%, indicating high resistance to NaCl DW-A.

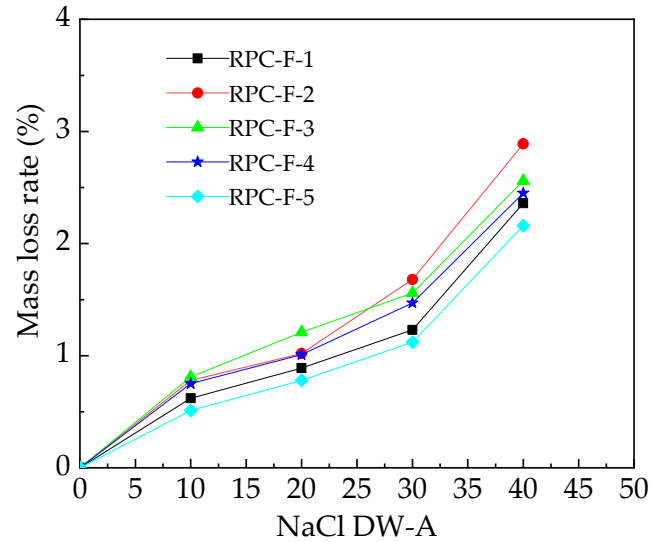


Figure 9. Mass loss rate during NaCl DW-A.

The RDEM of RPC after suffering from 0, 10, 20, and 30 NaCl DW-A is illustrated in Figure 10. It can be observed in Figure 10, the RDEM descends with the increasing number of NaCl DW-A. The main reason is attributed to the increasing and widening of cracks in the inner RPC by NaCl DW-A resulting in the decreased RDEM [33]. After the NaCl DW-A, the RDEM decreases in the following order: RPC with 0.5% basalt fibers + 1.5% steel fibers > RPC with 2% steel fibers > RPC with 3% basalt fibers > RPC with 2% basalt fibers > RPC with 3% steel fibers. This is mainly because the mechanical properties of steel fibers are higher than basalt fibers [34]. However, excessive steel fibers will accelerate the steel fibers' corrosion and increase cracks, leading to decreasing the RDEM. Therefore, when the steel fiber content is 3%, the RDEM of RPC is the lowest, while the RPC with 0.5% basalt fibers + 1.5% steel fibers shows the highest RDEM. The RDEM of RPC after suffering 30 NaCl DW-A is 82.1%~90.2%, showing perfect performance after NaCl DW-A action.

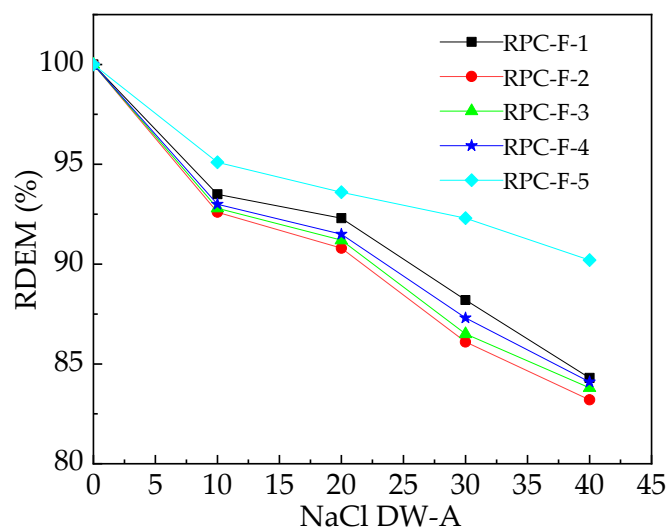
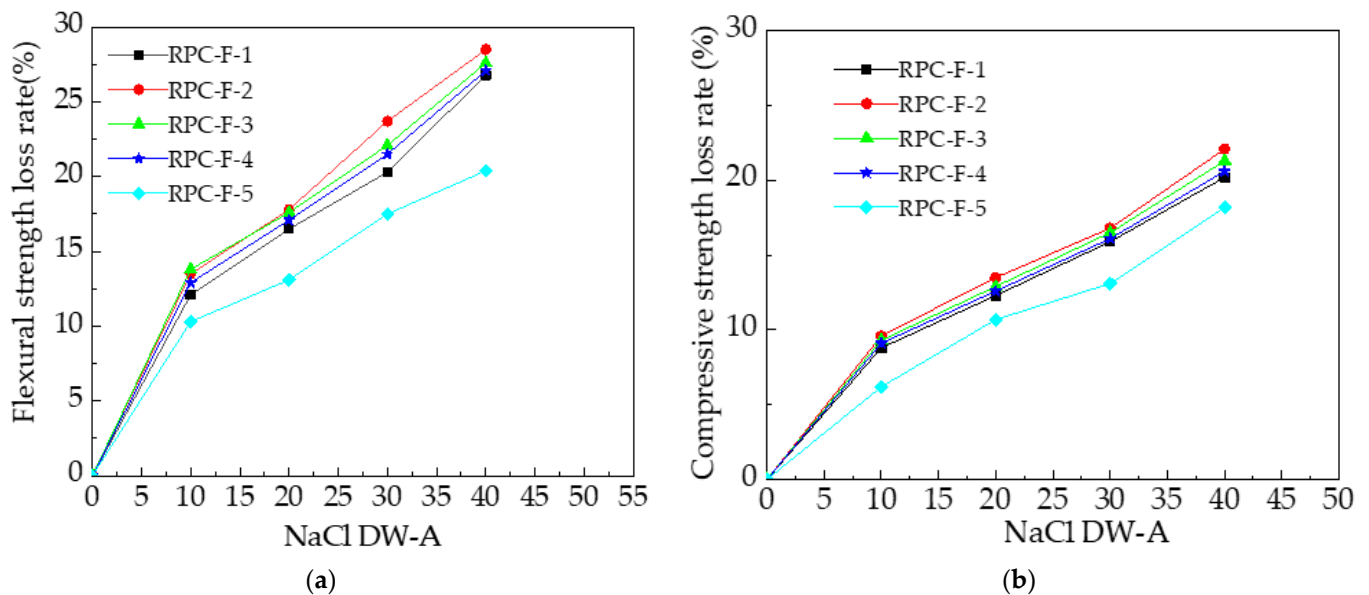


Figure 10. The RDEM of RPC during NaCl DW-A.

### 3.2.2. Mechanical Strength Loss Rates after NaCl DW-A

The mechanical strength loss rates after different NaCl DW-A are shown in Figure 11. As observed in Figure 11, mechanical strength loss rates increase with the number of NaCl DW-A. The mechanical strengths' loss rates are in accordance with the following order: RPC with 0.5% basalt fibers + 1.5% steel fibers < RPC with 2% steel fibers < RPC with 3% basalt fibers < RPC with 2% basalt fibers < RPC with 3% steel fibers. The reason for this phenomenon is that the assembly unit of basalt fibers and steel fibers is the best for reinforcing the mechanical strengths of RPC. The tensile strength of steel fibers is higher than that of basalt fibers. However, massive dosages of steel fibers accelerate the corrosion of steel fibers, leading to a reduction in the RPC's mechanical strength. As can be observed from Figure 11, the flexural strength loss rate of RPC is higher than the compressive strength loss rate of RPC. Comparing the mass loss rates and mechanical strength loss rates of the RPC exposed to NaCl DW-A with that of the RPC exposed to NaCl FT-C, the RPC shows higher resistance to NaCl FT-C than resistance to NaCl DW-A. The flexural and compressive strength loss rates are 20.4 %~28.5% and 18.2 %~22.1%.



**Figure 11.** Mechanical strength loss rates after NaCl DW-A. (a) Flexural strength loss rate (b) Compressive strength loss rate.

### 3.2.3. CMC during NaCl DW-A

The CMC of RPC after 0, 10, 20, and 30 NaCl DW-A is shown in Figure 12. As obtained from Figure 12, the CMC increases with the increasing NaCl DW-A. It is mainly because the cracks caused by the NaCl DW-A increase the probability of chloride ion diffusion, leading to the increase in CMC. The CMC after NaCl DW-A varies in the following order: RPC with 3% steel fibers > RPC with 2% steel fibers > RPC with 2% basalt fibers > RPC with 3% basalt fibers > RPC with 0.5% basalt fibers + 1.5% steel fibers. When 30 NaCl DW-A are finished, the CMC is  $1.6 \times 10^{-12} \sim 3.1 \times 10^{-12}$  ( $\text{m}^2/\text{s}$ ).

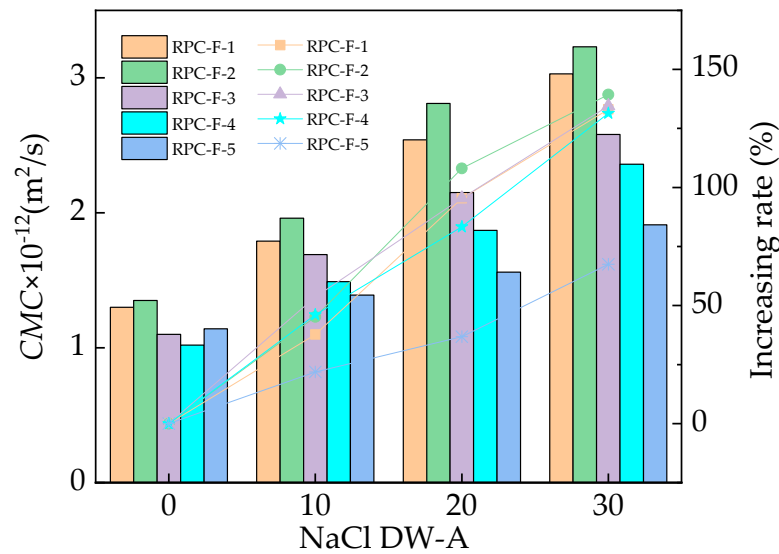


Figure 12. The CMC of RPC during NaCl DW-A.

### 3.2.4. Impact Toughness during NaCl DW-A

The impact toughness of RPC after different NaCl DW-A is illustrated in Figure 13. As depicted in Figure 13, the impact toughness decreases obviously with the increasing NaCl DW-A. This is mainly because that the cyclic crystallization stress of RPC is generated in the process of NaCl DW-A [35]. Hence, the cracks in RPC will expand, resulting in reducing the impact toughness. The reduction rate of impact toughness due to the NaCl DW-A coincides with the following order: RPC with 3% steel fibers > RPC with 2% steel fibers > RPC with 2% basalt fibers > RPC with 3% basalt fibers > RPC with 0.5% basalt fibers + 1.5% steel fibers. This is mainly because the passive film of steel fibers is corroded by chloride ions under the alternating action of NaCl DW-A, which leads to a rapid reduction in impact toughness [36]. Comparing Figures 8 and 13, the impact toughness of RPC after NaCl FT-C is higher than that after NaCl DW-A. After 30 NaCl DW-A, the impact toughness is 678~2471 J.

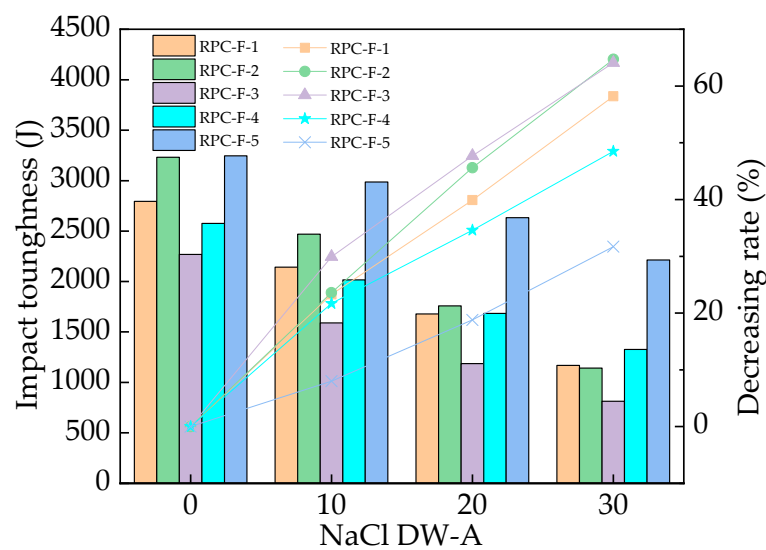


Figure 13. The impact toughness of RPC during NaCl DW-A.

Comparing the results of our research with those of other researchers [25,27], the mass loss rates, RDEM, mechanical strength loss rates and CMC of the RPC with an assembly

unit of steel fibers and basalt fibers after 30 NaCl DW-A are 79.8%~86.1%, 123.1%~135.2%, 83.6%~88.1% and are 92.3%~94.5% in the RPC with mono-doped basalt fibers or steel fibers.

#### 4. Conclusions

The conclusion of the research can be summarized as follows.

The mass loss rates, the mechanical strength loss rates and CMC are increased by the actions of NaCl FT-C and DW-A. Meanwhile, the NaCl FT-C and DW-A lead to decreased RDEM and impact toughness.

The addition of BFs and SFs can improve mechanical performances and resistance to NaCl actions. The NaCl erosion resistance of the RPC accords with the following order: RPC with 0.5% basalt fibers + 1.5% steel fibers > RPC with 2% steel fibers > RPC with 3% basalt fibers > RPC with 2% basalt fibers > RPC with 3% steel fibers. Specimens with 0.5% basalt fibers and 1.5% steel fibers show the optimum mechanical strength and the resistance to NaCl erosion.

The mass loss rates, RDEM, flexural strength loss rate, compressive strength loss rate, CMC and impact toughness of all specimens after 300 NaCl FT-C are 1.62%~4.5%, 83.2%~91.7%, 22.3%~36.7% and 15.7%~28.1%,  $1.1 \times 10^{-12}$ ~ $3.2 \times 10^{-12}$  (m<sup>2</sup>/s) and 625~2456 J, while the corresponding parameters of specimens after 40 NaCl DW-A are 2.1%~3.2%, 82.1%~90.2%, 20.4%~28.5%, 18.2%~22.1%,  $1.6 \times 10^{-12}$ ~ $3.1 \times 10^{-12}$  (m<sup>2</sup>/s) and 678~2471 J. According to comprehensive comparisons, these properties decay more seriously after 300 NaCl FT-C.

The goal of this study is to provide a kind of concrete material with ultra-high mechanical strength and durability for marine structures.

**Author Contributions:** Conceptualization, Z.C. and H.W.; methodology, J.R.; software, C.J.; validation, Z.C., H.W. and G.S.; formal analysis, X.G.; investigation, W.C.; resources, H.W.; data curation, Z.C.; writing—original draft preparation, Z.C.; writing—review and editing, H.W.; visualization, J.R.; supervision, Z.C.; project administration, H.W.; funding acquisition, H.W. All authors have read and agreed to the published version of the manuscript.

**Funding:** This research was funded by Zhejiang Provincial Natural Science Foundation [No. LY22E080005].

**Institutional Review Board Statement:** Not applicable.

**Informed Consent Statement:** Not applicable.

**Data Availability Statement:** Not applicable.

**Conflicts of Interest:** The authors declare no conflict of interest.

#### References

- Dong, S.F.; Li, L.W.; Ashour, A.; Dong, X.F.; Han, B.G. Self-assembled 0D/2D nano carbon materials engineered smart and multifunctional cement-based composites. *Constr. Build. Mater.* **2021**, *272*, 121632. [\[CrossRef\]](#)
- Li, Y.; Li, X.; Tan, Y. Effect of aging on fatigue performance of cement emulsified asphalt repair material. *Constr. Build. Mater.* **2021**, *292*, 123417. [\[CrossRef\]](#)
- Ju, Y.; Zhao, J.; Wang, D.; Song, Y. Experimental study on flexural behaviour of reinforced reactive powder concrete pole. *Constr. Build. Mater.* **2021**, *312*, 125399. [\[CrossRef\]](#)
- Rajasekar, A.; Arunachalam, K.; Kottaisamy, M. Durability of ultra-high strength concrete with waste granite sand as partial substitute for aggregate. *J. Comput. Theor. Nanosci.* **2018**, *15*, 446–452. [\[CrossRef\]](#)
- Shen, W.G.; Liu, Y.; Cao, L.G.; Huo, X.J.; Yang, Z.G.; Zhou, C.C.; He, P.T.; Lu, Z.L. Mixing design and microstructure of ultra-high strength concrete with manufactured sand. *Constr. Build. Mater.* **2017**, *143*, 312–321. [\[CrossRef\]](#)
- Shan, B.; Lai, D.D.; Xiao, Y.; Luo, X.B. Experimental research on concrete-filled RPC tubes under axial compression load. *Eng. Struct.* **2018**, *155*, 358–370. [\[CrossRef\]](#)
- Haselbach, L.; Valavala, S.; Montes, F. Permeability predictions for sand clogged Portland cement pervious concrete pavement systems. *J. Environ. Manag.* **2005**, *81*, 42–49. [\[CrossRef\]](#) [\[PubMed\]](#)
- Li, S.Q.; Feng, Y.C.; Yang, J.B.; Cerny, R. Expansion mechanism and properties of magnesium oxide expansive hydraulic cement for engineering applications. *Adv. Mater. Sci. Eng.* **2021**, *2021*, 5542072. [\[CrossRef\]](#)
- Yoo, D.Y.; Banthia, N.; Lee, J.Y.; Yoon, Y.S. Effect of fiber geometric property on rate dependent flexural behavior of ultra-high-performance cementitious composite. *Cem. Concr. Compos.* **2018**, *86*, 57–71. [\[CrossRef\]](#)

10. Dong, S.; Wang, Y.; Ashour, A.; Han, B.G.; Ou, J.P. Uniaxial compressive fatigue behavior of ultra-high performance concrete reinforced with super-fine stainless wires. *Int. J. Fatigue* **2021**, *142*, 105959. [[CrossRef](#)]
11. Heng, K.; Jia, P.C.; Xu, J.P.; Li, R.W.; Wu, H. Vehicular impact resistance of highway bridge with seismically-designed UHPC pier. *Eng. Struct.* **2022**, *252*, 113635. [[CrossRef](#)]
12. Zhu, J.; Liu, S.; Song, L.; Qu, Z.; Wang, H. Influence of Carbon Dioxide Curing on the Corrosion Resistance of Reinforced Cement Mortar under the External Erosion of NaCl Freeze–Thaw Cycle. *Appl. Sci.* **2022**, *12*, 5061. [[CrossRef](#)]
13. Tan, C.J.; Zhang, Y.; Zhao, H.; Zhang, B.; Du, T. Study on Shear-Lag Effect of Steel–UHPC Ribbed Slab Composite Structures Using Bar Simulation Method. *Buildings* **2022**, *12*, 1884. [[CrossRef](#)]
14. Wang, H.; Liu, X.; Yue, Q.; Wang, N.; Zheng, M.Z. Longitudinal shear behavior and design method of UHPC connection for prefabricated slabs in composite beams. *Eng. Struct.* **2023**, *277*, 115386. [[CrossRef](#)]
15. Wang, H.; Zhang, A.; Zhang, L.; Wang, Q.; Yang, X.; Gao, X.; Shi, F. Electrical and piezoresistive properties of carbon nanofiber cement mortar under different temperatures and water contents. *Constr. Build. Mater.* **2020**, *265*, 120740. [[CrossRef](#)]
16. Zhao, X.; Cai, L.; Ji, X.H.; Zeng, W.; Liu, J.T. Mechanical Properties of Polyethylene Fiber Reinforced Ultra High Performance Concrete (UHPC). *Materials*. **2022**, *15*, 8374. [[CrossRef](#)]
17. Zhang, Y.; Li, X.L.; Zhu, Y.P.; Shao, X.D. Experimental study on flexural behavior of damaged reinforced concrete (RC) beam strengthened by toughness-improved ultra-high performance concrete (UHPC) layer. *Composites Part B* **2020**, *186*, 107834. [[CrossRef](#)]
18. Sohn, Y.S.; Lee, J.H.; Lee, S.H. Fire resistance of hybrid fibre-reinforced, ultra-high-strength concrete columns with compressive strength from 120 to 200 MPa. *Mag. Concr. Res.* **2012**, *64*, 539–550.
19. Wang, H.; Gao, X.; Liu, J.; Ren, M.; Lu, A. Multi-functional properties of carbon nanofiber reinforced reactive powder concrete. *Constr. Build. Mater.* **2018**, *187*, 699–707. [[CrossRef](#)]
20. Alhoubi, Y.; Mahaini, Z.; Abed, F. The Flexural Performance of BFRP-Reinforced UHPC Beams Compared to Steel and GFRP-Reinforced Beams. *Sustainability* **2022**, *14*, 15139. [[CrossRef](#)]
21. Sun, M.; Visintin, P.; Bennett, T. The effect of specimen size on autogenous and total shrinkage of ultra-high performance concrete (UHPC). *Constr. Build. Mater.* **2022**, *327*, 126952. [[CrossRef](#)]
22. Huang, G.; Wang, H.; Shi, F. Coupling Effect of Salt Freeze–Thaw Cycles and Carbonation on the Mechanical Performance of Quick Hardening Sulphoaluminate Cement-Based Reactive Powder Concrete with Basalt Fibers. *Coatings* **2021**, *11*, 1142. [[CrossRef](#)]
23. Wang, H.; Jin, K.; Zhang, A.; Zhang, L.; Han, Y.; Liu, J.; Shi, F.; Feng, L. External erosion of sodium chloride on the degradation of self-sensing and mechanical properties of aligned stainless steel fiber reinforced reactive powder concrete. *Constr. Build. Mater.* **2021**, *287*, 123028. [[CrossRef](#)]
24. Shi, X.; Fay, L.; Peterson, M.; Yang, Z. Freeze-thaw damage and chemical change of a portland cement concrete in the presence of diluted deicers. *Mater. Struct.* **2010**, *43*, 933–946. [[CrossRef](#)]
25. Cai, Z.; Wang, H. Influence of NaCl Freeze–thaw Cycles on the Mechanical Strength of Reactive Powder Concrete with the Assembly Unit of Sulphoaluminate Cement and Ordinary Portland Cement. *Coatings* **2021**, *11*, 1238. [[CrossRef](#)]
26. Cao, H.; Liang, Z.; Peng, X.; Cai, X.; Wang, K.; Wang, H.; Lyu, Z. Research of Carbon Dioxide Curing on the Properties of Reactive Powder Concrete with Assembly Unit of Sulphoaluminate Cement and Ordinary Portland Cement. *Coatings* **2022**, *12*, 209. [[CrossRef](#)]
27. Hong, X.; Wang, H.; Shi, F. Influence of NaCl freeze thaw cycles and cyclic loading on the mechanical performance and permeability of sulphoaluminate cement reactive powder concrete. *Coatings* **2020**, *10*, 1227. [[CrossRef](#)]
28. Qiang, L.; Ibrahim, L.; Zhou, W.; Zhang, M.; Yuan, Z. Treatment methods for plant fibers for use as reinforcement in cement-based materials. *Cellulose* **2021**, *28*, 5257–5268.
29. Zhong, S.; Fu, J. Surface modification of copper-plated steel fiber and its corrosion resistance and bonding properties. *J. Build. Mater.* **2019**, *22*, 606–610.
30. Liang, X.; Kang, J.; Chen, J.; Geng, L.; You, Z. Mechanical properties test of copper-coated steel fiber lightweight aggregate concrete. *J. North China Univ. Sci. Technol.* **2021**, *43*, 32–37.
31. Zhu, J.; Qu, Z.; Liang, S.; Li, B.; Du, T.; Wang, H. The macro-scopic and microscopic properties of cement paste with carbon dioxide curing. *Materials* **2022**, *15*, 1578. [[CrossRef](#)] [[PubMed](#)]
32. Wang, H.; Zhang, A.; Zhang, L.; Liu, J.; Han, Y.; Wang, J. Research on the Influence of Carbonation on the Content and State of Chloride Ions and the Following Corrosion Resistance of Steel Bars in Cement Paste. *Coatings* **2020**, *10*, 1071. [[CrossRef](#)]
33. Liang, J.; Zhu, H.; Chen, L.; Han, X.; Guo, Q.; Gao, Y.; Liu, C. Rebar corrosion investigation in rubber aggregate concrete via the chloride electro-accelerated test. *Materials* **2019**, *12*, 862. [[CrossRef](#)]
34. Xu, Q.; Ji, T.; Yang, Z.; Ye, Y. Steel rebar corrosion in artificial reef concrete with sulphoaluminate cement, sea water and marine sand. *Constr. Build. Mater.* **2019**, *227*, 116685. [[CrossRef](#)]

35. Wang, J.; Chen, Z.; Wu, K. Properties of calcium sulfoaluminate cement made ultra-high performance concrete: Tensile performance, acoustic emission monitoring of damage evolution and microstructure. *Constr. Build. Mater.* **2019**, *208*, 767–779. [[CrossRef](#)]
36. Keshavarzian, F.; Saberian, M.; Li, J. Investigation on mechanical properties of steel fiber reinforced reactive powder concrete containing nano-SiO<sub>2</sub>: An experimental and analytical study. *J. Build. Eng.* **2021**, *44*, 102601. [[CrossRef](#)]

**Disclaimer/Publisher's Note:** The statements, opinions and data contained in all publications are solely those of the individual author(s) and contributor(s) and not of MDPI and/or the editor(s). MDPI and/or the editor(s) disclaim responsibility for any injury to people or property resulting from any ideas, methods, instructions or products referred to in the content.